Highly specular carbon nanotube absorbers

X. J. Wang, L. P. Wang, O. S. Adewuyi, B. A. Cola, and Z. M. Zhang[a)]
G. W. Woodruff School of Mechanical Engineering, Georgia Institute of Technology, Atlanta, Georgia 30332, USA

(Received 13 August 2010; accepted 25 September 2010; published online 21 October 2010)

Specular black materials have important applications, such as in absolute cryogenic radiometers, space-borne spectroradiometers, and some energy conversion devices. While vertically aligned carbon nanotubes (VACNT) can have close-to-unity absorptance, so far the reported reflection has been essentially diffuse. This letter describes a highly specular black absorber made of VACNT. Both the bidirectional reflectance distribution function and specular reflectance were measured at the wavelength $\lambda=635$ nm using a laser scatterometer. The ordinary and extraordinary optical constants were obtained by fitting the specular reflectance, calculated from modified reflectance formulae for light incident from air to a uniaxial medium, considering surface roughness. Furthermore, the absorptance at $\lambda=635$ nm was shown to be 0.994 ± 0.002, based on the measured directional-hemispherical reflectance. © *2010 American Institute of Physics*.
[doi:10.1063/1.3502597]

Black materials have numerous applications, e.g., efficient absorbers or emitters for energy conversion, stray light shields and detector coatings in optical systems, and radiometers or sensors in space-borne infrared systems.[1–9] High absorptance can be achieved using vertically aligned carbon nanotubes (VACNT) due to their low effective refractive index.[10–16] There are two types of black surfaces: highly specular or glossy and nearly diffuse or matte. In certain applications, such as blackbody cavities for absolute radiometry, radiation thermometry, and baffle design, specular black is often preferred over diffuse black.[4,9,17] Furthermore, to better understand the effective optical constants, samples with relatively smooth surfaces are desirable. Thus far the reported CNT arrays with high absorptance are all diffuse like, due to surface roughness and other inhomogeneity.[10–12,18,19] This letter reports an optical study of VACNT with high absorptance and specular reflection.

Multiwall VACNT specimens were synthesized on a 100-mm-diameter Si wafer using a thermal chemical vapor deposition method. The catalysts were made by coating a trilayer of 30 nm Ti, 10 nm Al, and 3 nm Fe in sequence.[20] Process gases of C_2H_2 and H_2 were used with different flow rates in a N_2 carrier gas. During CNT growth, the substrate temperature was 750 °C and the growth pressure was 70 kPa. Based on scanning electron microscopy (SEM) images, the array height was determined to be (166 ± 16) μm. The surface area of the substrate and the weight of CNTs scraped from the substrate were measured to estimate the array density, which was (0.067 ± 0.010) g/cm^3. Hence, the volume fraction was calculated to be approximately 3% using the graphite density of 2.2 g/cm^3 for CNTs. More discussions on the fabrication and characterization were presented elsewhere.[21] The SEM images are depicted in Fig. 1. Figure 1(c) with low magnification suggests that the CNTs are highly aligned with a uniform height. The high-resolution image shown in Fig. 1(a) demonstrates good alignment near the tip. Figure 1(b) was taken from the middle region and some bending and entanglement of tubes can be seen. The sample surface appears shiny and displays different colors at grazing angles. This may be due to interference and diffraction effects caused by surface roughness, tip scattering, and optical anisotropy, though the exact reason needs further investigation. Atomic force microscopy (AFM) was used to obtain the surface profile of the CNT array, and the rms roughness was $\sigma_{rms}=57$ nm with a scanning area of 10×10 μm^2.

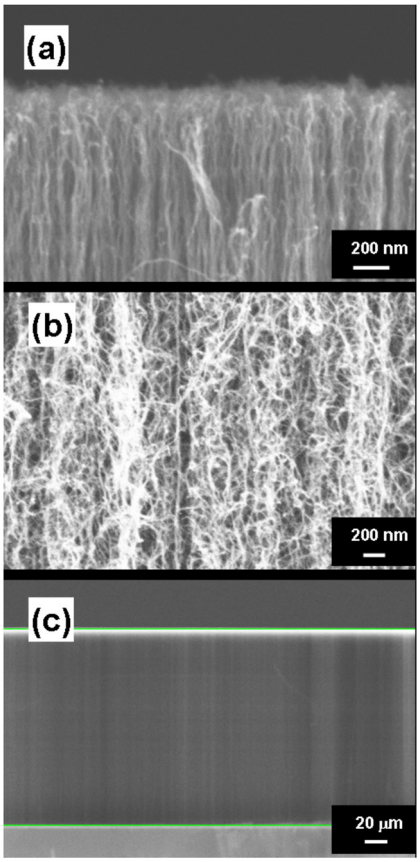

FIG. 1. (Color online) SEM images of the CNT array: (a) top region; (b) middle region; (c) entire CNT layer, the average height is 166 μm.

[a)]Electronic mail: zhuomin.zhang@me.gatech.edu. Tel.: (404) 385-4225. FAX: (404) 894-8496.

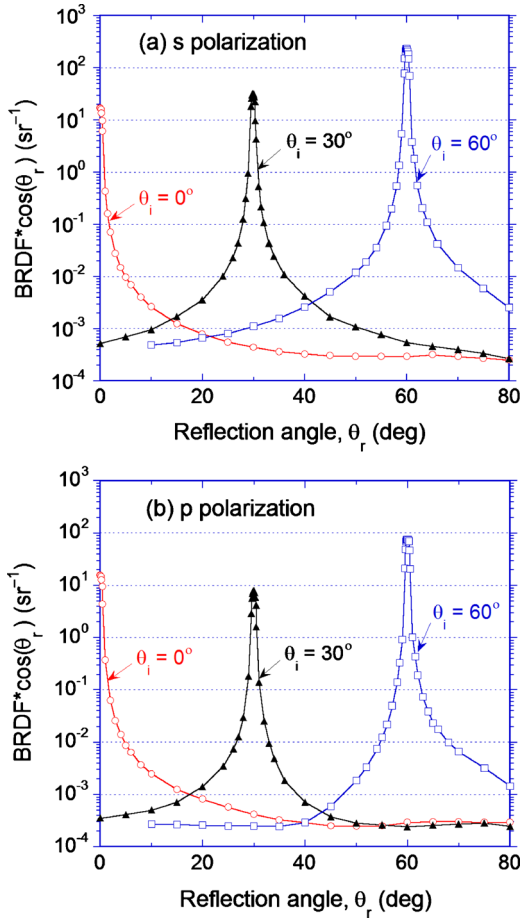

FIG. 2. (Color online) Measured BRDFs of the specular CNT array at $\lambda=635$ nm for different incidence angles: (a) *s* polarization; (b) *p* polarization.

A laser scatterometer was used to measured the bidirectional reflectance distribution function (BRDF), defined as the ratio of the reflected radiance to the incident irradiance, with a diode laser of $\lambda=635$ nm.[22] During the measurement, the laser beam was linearly polarized before reaching the sample. For in-plane BRDF measurements, the sample and a silicon detector were rotated independently along the same axis to vary the angles of incidence θ_i and reflection (or scattering) θ_r individually. The detection solid angle was $\Delta\omega_r=1.84\times10^{-4}$ sr, resulting in a half cone angle of 0.45° to resolve the specular peak and angular distributions. Precautions were applied to reduce stray light and to improve the signal-to-noise ratio for low-level measurements.[21,23]

The BRDF measurement results are shown in Fig. 2, in which the ordinate is the product BRDF$\times\cos\theta_r$, often called the cosine corrected BRDF, which is proportional to the power received by the detector. Also, the cosine corrected BRDF is proportional to the power that the detector received for given incidence power and solid angle. Each curve corresponds to a fixed θ_i for individual polarization, while θ_r is varied at an increment of 5°, except around the specular peak where the interval is 0.2°. For normal incidence, the BRDF exhibits symmetry on both sides and the average is used to present θ_r from 3° to 80°. Within 3° scattering angle, the BRDF could not be measured because the detector would block the incoming beam. To resolve the specular peak at normal incidence, θ_i was set to 4° and the specular peak was shifted by 4° in θ_r to match up with the off-peak BRDF at $\theta_i=0°$. The uncertainty in the BRDF is estimated to be 10% near the specular peak when BRDF$\times\cos\theta_r$ is about 10 sr^{-1}, but increases to 40% when the corrected BRDF is less than 0.001 sr^{-1} due to low signal-to-noise ratio and stray light.

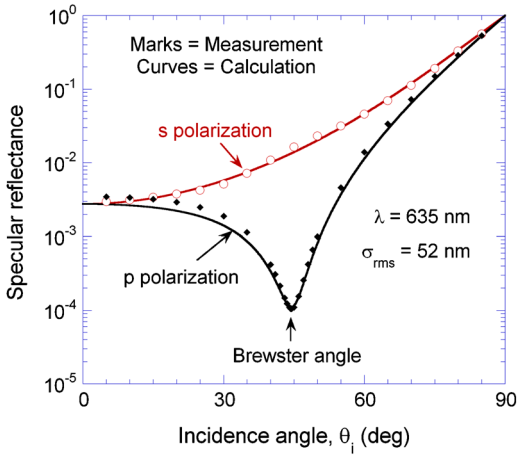

FIG. 3. (Color online) Measured and calculated (with best fitted parameters) specular reflectance vs incidence angle.

From Fig. 2, very high and sharp specular peaks exist for all incidence angles and polarizations. The corrected BRDF drops for about five orders of magnitude away from the peak. The width and sharpness for this CNT sample are comparable with those measured for Chemglaze Z302, commonly used in high-accuracy radiometers.[3,4] However, the measured BRDF away from the specular peak is two to four times lower than that of Chemglaze Z302, suggesting that the CNT array has a lower directional-hemispherical reflectance (R_{dh}) or higher absorptance. Also, the peak magnitudes are higher for *s* polarization than for *p* polarization at $\theta_i=30°$ and 60°; this is consistent with the reflection characteristics (i.e., Fresnel reflection) for a smooth interface. The BRDF peak is the lowest for *p* polarization at $\theta_i=30°$, because it is close to the Brewster angle to be discussed later.

The specular reflectance was measured with the same instrument by setting $\theta_r=\theta_i$ based on the ratio of the reflected signal to the incident signal. The laser beam diameter was approximately 3 mm, and the detector aperture was 8 mm in diameter to fully capture the specular reflection. The measurements were taken at various incidence angles from 5° to 80° with an interval of 5°. The measurements (marks) and calculation (curves) are shown in Fig. 3. While the specular reflectance increases monotonically with θ_i for *s* polarization, it reaches a minimum at the Brewster angle of 44° for *p* polarization. Notice that the Brewster angle between two isotropic media must be greater than 45° for incidence from the optically rarer medium. At the Brewster angle, the specular reflectance can be as small as 0.0001. The CNT array may be treated as an effective uniaxial medium, whose optical constants are $\tilde{N}_o=n_o+ik_o$ for ordinary rays and $\tilde{N}_e=n_e+ik_e$ for extraordinary rays.

In order to determine the effective $\tilde{N}_o$ and $\tilde{N}_e$, the reflectance for incidence from air to a uniaxial medium is calculated using the following expressions:[24,25]

$$R_s=\left(\frac{\cos\theta_i-\sqrt{\tilde{N}_o^2-\sin^2\theta_i}}{\cos\theta_i-\sqrt{\tilde{N}_o^2-\sin^2\theta_i}}\right)^2 C_{sp}, \quad \text{for } s \text{ polarization}, \quad (1)$$

$$\text{and} \quad R_p = \left(\frac{\tilde{N}_o \tilde{N}_e \cos\theta_i - \sqrt{\tilde{N}_e^2 - \sin^2\theta_i}}{\tilde{N}_o \tilde{N}_e \cos\theta_i + \sqrt{\tilde{N}_e^2 - \sin^2\theta_i}} \right)^2 C_{sp}, \quad \text{for } p \text{ polarization}, \tag{2}$$

where $C_{sp}=\exp[-16\pi^2\sigma_{rms}^2 \cos^2(\theta_i)/\lambda^2]$ accounts for scattering loss and is called the specularity parameter.[26,27]

A least-squares method is applied to find the minimal relative difference between the calculated and measured reflectance, as described by the objective function, as follows:

$$F = \sqrt{\frac{1}{N}\sum_{j=1}^{N} \left(\frac{R_{cal,j} - R_{meas,j}}{R_{meas,j}} \right)^2} \tag{3}$$

where subscripts "cal" and "meas" stand for calculated and measured, j is the data point for each incidence angle, and N is the total number of measurements. The procedure begins by taking $\tilde{N}_o$ and σ_{rms} as adjustable parameters to fit the measured reflectance for s polarization. The fitted $\tilde{N}_o$ and σ_{rms} are used along with Eq. (2) to minimize the objective function for p-polarized reflectance in order to obtain $\tilde{N}_e$. The best fitting gives the smallest objective function, $F=7\%$ for s polarization and $F=15\%$ for p polarization. The values obtained from fitting are $n_o=1.19\pm0.03$, $k_o=0.043\pm0.009$, $n_e=1.33\pm0.08$, $k_e=0.03\pm0.01$, and $\sigma_{rms}=52\pm10$ nm. The uncertainties are estimated based on a 10% variation for s polarization and 20% variation for p polarization as the error bounds of the objective function. Note that the fitted rms roughness agrees well with that measured from AFM (57 nm). The parameter C_{sp} increases with θ_i and varies from 0.35 at $\theta_i=0°$ to 0.90 at $\theta_i=72°$ with $\sigma_{rms}=52$ nm. Based on the fitted extinction coefficients, the radiation penetrate depth is less than 2 μm, which is much smaller than the average height of the CNTs. Hence, it is appropriate to treat the CNT array as a semi-infinite medium.

The effective medium theory (EMT) has been used to explain the low refractive index of CNT arrays.[28–30] While the values of optical constants obtained by fitting fall in the range predicted by EMT, it is difficult to quantitatively predict $\tilde{N}_o$ and $\tilde{N}_e$ using EMT because the misalignment and nonuniformity of the CNT arrays and the lack of knowledge of the inherent dielectric function and structure of the multiwall CNTs.[12,19] While the polarization-dependent absorption of CNTs has been studied for thin CNT arrays, the focus in these studies was on the anisotropic absorption cross-section without considering the surface roughness effect.[31,32]

The R_{dh} of the CNT array was also measured using an integrating sphere. The measured R_{dh} at $\lambda=635$ nm is 0.0058 ± 0.0018, which agrees reasonably well with 0.0064 ± 0.0026 as calculated by integrating the BRDF at normal incidence, assuming isotropy in the azimuth direction. The absorptance, $1-R_{dh}$, at 635 nm is estimated to be 0.994 with a relative uncertainty of 0.2%. Furthermore, the absorptance varies from 0.995 to 0.997 at wavelengths from 400 to 1000 nm.[21]

In summary, VACNT can be made as a highly specular black material, as demonstrated by the sharp peaks in the measured BRDF. It is shown that the CNT array can be considered as an effective homogeneous uniaxial medium. The ordinary and extraordinary optical constants are quantitatively obtained from the measured specular reflectance for individual polarizations. The rms roughness obtained by fitting the specular reflectance agrees with the AFM measurement. This study not only suggests a method for determining the anisotropic optical constants and surface roughness of VACNT, but also opens up opportunities in applying VACNT to absolute radiometry and space-borne spectrometry.

X.J.W., L.P.W., and Z.M.Z. thank the support of NSF (Grant No. CBET-0828701). O.S.A. and B.A.C. appreciate support from the DARPA NTI program, Georgia Tech startup funds, and Georgia Tech's Nanotechnology Research Center. Thanks to Mr. Sheng Xu for help taking SEM images.

[1] M. J. Persky, Rev. Sci. Instrum. **70**, 2193 (1999).
[2] J.-Q. Xi, M. F. Schubert, J. K. Kim, E. F. Schubert, M. Chen, S.-Y. Lin, W. Liu, and J. A. Smart, Nat. Photonics **1**, 176 (2007).
[3] K. A. Snail, D. P. Brown, J. Costantino, W. C. Shemano, C. W. Schmidt, W. F. Lynn, C. L. Seaman, and T. R. Knowles, Proc. SPIE **2864**, 465 (1996).
[4] R. U. Datla, K. Stock, A. C. Parr, C. C. Hoyt, P. J. Miller, and P. V. Foukal, Appl. Opt. **31**, 7219 (1992).
[5] D. B. Betts, F. J. J. Clarke, L. J. Cox, and J. A. Larkin, J. Phys. E **18**, 689 (1985).
[6] T. E. Wightman and F. Grum, Color Res. Appl. **6**, 139 (1981).
[7] J. Zhu, Z. Yu, G. F. Burkhard, C. M. Hsu, S. T. Connor, Y. Xu, Q. Wang, M. McGehee, S. Fan, and Y. Cui, Nano Lett. **9**, 279 (2009).
[8] R. Yan, D. Gargas, and P. Yang, Nat. Photonics **3**, 569 (2009).
[9] *Radiometric Temperature Measurements: I & II*, edited by Z. M. Zhang, B. K. Tsai, and G. Machin (Academic, New York, 2010).
[10] Z.-P. Yang, L. Ci, J. A. Bur, S.-Y. Lin, and P. M. Ajayan, Nano Lett. **8**, 446 (2008).
[11] K. Mizuno, J. Ishii, H. Kishida, Y. Hayamizu, S. Yasuda, D. N. Futaba, M. Yumura, and K. Hata, Proc. Natl. Acad. Sci. U.S.A. **106**, 6044 (2009).
[12] X. J. Wang, J. D. Flicker, B. J. Lee, W. J. Ready, and Z. M. Zhang, Nanotechnology **20**, 215704 (2009).
[13] R. E. Camacho, A. R. Morgan, M. C. Flores, T. A. McLeod, V. S. Kumsomboone, B. J. Mordecai, R. Bhattacharjea, W. Tong, B. K. Wagner, J. D. Flicker, S. P. Turano, and W. J. Ready, JOM **59**, 39 (2007).
[14] P. Avouris, M. Freitag, and V. Perebeinos, Nat. Photonics **2**, 341 (2008).
[15] J. H. Lehman, R. Deshpande, P. Rice, B. To, and A. C. Dillon, Infrared Phys. Technol. **47**, 246 (2006).
[16] J. Lehman, A. Sanders, L. Hanssen, B. Wilthan, J. Zeng, and C. Jensen, Nano Lett. **10**, 3261 (2010).
[17] G. L. Peterson, S. C. Johnston, and J. Thomas, Proc. SPIE **1753**, 65 (1992).
[18] I. Ivanov, A. Puretzky, G. Eres, H. Wang, Z. Pan, H. Cui, R. Jin, J. Howe, and D. B. Geohegan, Appl. Phys. Lett. **89**, 223110 (2006).
[19] K. Ramadurai, C. L. Cromer, L. A. Lewis, K. E. Hurst, A. C. Dillon, R. L. Mahajan, and J. H. Lehman, J. Appl. Phys. **103**, 013103 (2008).
[20] J. Xu and T. S. Fisher, Int. J. Heat Mass Transfer **49**, 1658 (2006).
[21] X. J. Wang, O. S. Adewuyi, L. P. Wang, B. A. Cola, and Z. M. Zhang, Proc. SPIE **7792**, 77920R (2010).
[22] Y. J. Shen, Q. Z. Zhu, and Z. M. Zhang, Rev. Sci. Instrum. **74**, 4885 (2003).
[23] H. J. Lee and Z. M. Zhang, Int. J. Thermophys. **27**, 820 (2006).
[24] P. Yeh, *Optical Waves in Layered Media* (Wiley, New York, 1988).
[25] C. G. Malone, B. I. Choi, M. I. Flik, and E. G. Cravalho, J. Heat Transfer **115**, 1021 (1993).
[26] Y. J. Shen, Z. M. Zhang, B. K. Tsai, and D. P. DeWitt, Int. J. Thermophys. **22**, 1311 (2001).
[27] Z. M. Zhang, *Nano/Microscale Heat Transfer* (McGraw-Hill, New York, 2007).
[28] F. J. García-Vidal, J. M. Pitarke, and J. B. Pendry, Phys. Rev. Lett. **78**, 4289 (1997).
[29] X. H. Wu, L. S. Pan, H. Li, X. J. Fan, T. Y. Ng, D. Xu, and C. X. Zhang, Phys. Rev. B **68**, 193401 (2003).
[30] T. de los Arcos, P. Oelhafen, and D. Mathys, Nanotechnology **18**, 265706 (2007).
[31] Y. Murakami, E. Einarsson, T. Edamura, and S. Maruyama, Phys. Rev. Lett. **94**, 087402 (2005).
[32] C. Ni and P. R. Bandaru, Carbon **47**, 3054 (2009).